Silicon Decorated with Amorphous Cobalt Molybdenum Sulfide Catalyst as an Efficient Photocathode for Solar Hydrogen Generation

Yang Chen,[†,‡] Phong D. Tran,[*,†,‡] Pablo Boix,[†] Yi Ren,[§] Sing Yang Chiam,[§] Zhen Li,[†] Kunwu Fu,[†] Lydia H. Wong,[*,‡] and James Barber[‡,∥]

[†]Energy Research Institute at Nanyang Technological University (ERI@N), 50 Nanyang Drive, Singapore 637553, [‡]Solar Fuels Laboratory, Nanyang Technological University, 50 Nanyang Avenue, Singapore 639798, [§]Institute of Materials Research and Engineering, A*STAR (Agency for Science, Technology and Research), 3 Research Link, Singapore 117602, and [∥]Department of Life Science, Imperial College London, SW7 2AZ London, U.K.

ABSTRACT The construction of viable photoelectrochemical (PEC) devices for solar-driven water splitting can be achieved by first identifying an efficient independent photoanode for water oxidation and a photocathode for hydrogen generation. These two photoelectrodes then must be assembled with a proton exchange membrane within a complete coupled system. Here we report the preparation of a Si/*a*-$CoMoS_x$ hybrid photocathode which shows impressive performance (onset potential of 0.25 V *vs* RHE and photocurrent j_{sc} of 17.5 mA cm^{-2} at 0 V *vs* RHE) in pH 4.25 phosphate solution and under simulated AM 1.5 solar illumination. This performance is among the best reported for Si photocathodes decorated with noble-metal-free catalysts. The electrode preparation is scalable because it relies on a photoassisted electrodeposition process employing an available p-type Si electrode and $[Co(MoS_4)_2]^{2-}$ precursor. Investigation of the mechanism of the Si/*a*-$CoMoS_x$ electrode revealed that under conditions of H_2 photogeneration this bimetallic sulfide catalyst is highly efficient in extracting electrons from illuminated Si and subsequently in reducing protons into H_2. The Si/*a*-$CoMoS_x$ photocathode is functional over a wide range of pH values, thus making it a promising candidate for the construction of a complete solar-driven water splitting PEC device.

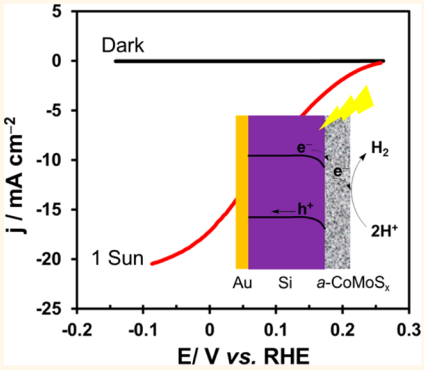

KEYWORDS: solar fuels · water splitting · catalysis · molybdenum sulfide · hydrogen

Solar-driven water splitting is a potential technology to produce large amounts of hydrogen which can then be used as a renewable fuel. Recent computational analysis shows that high solar-to-hydrogen conversion efficiency up to 28% can be achieved by employing a dual light absorber photoelectrochemical (PEC) cell.[1] The best simulated cell consists of a photocathode and a photoanode made of semiconductors with a band gap of ~1.0 and ~1.7 eV, respectively. Because the band gap of silicon is 1.1 eV and its theoretical maximum photocurrent is 44 mA cm^{-2}, it is an ideal candidate as a photocathode for PEC engineering.[2] However, kinetics of the hydrogen evolution reaction (HER) on the Si electrode surface is rather slow. To accelerate the H_2 generation process, decorating the Si electrode surface with an efficient HER catalyst is needed. So far, Pt is the best HER catalyst, and its implementation within a Si photocathode has been shown to induce an impressive enhancement of photocatalytic activities.[3−5] However, a cost-effective solar hydrogen production technology relying on precious materials like Pt is not feasible for large-scale operation.

Recent research efforts have identified several attractive noble-metal-free alternatives to Pt including metal alloys[4] and sulfides of transition metals.[6−14] Some of these catalysts have been successfully incorporated with Si photocathodes. Incorporation of crystalline molybdenum disulfide (*c*-MoS_2) or amorphous molybdenum sulfide (*a*-MoS_x) catalysts can be accomplished by different methodologies such as simple drop-casting,[15,16] electrodeposition,[17] or sulfidization of Mo.[5,18] Recently, we adapted the

* Address correspondence to dptran@ntu.edu.sg, lydiawong@ntu.edu.sg.

Received for review November 30, 2014 and accepted March 23, 2015.

Published online March 23, 2015
10.1021/nn506819m

electrodeposition method[8,19,20] for photoassisted deposition of *a*-MoS_x onto a semiconductor electrode (or nanoparticles) surface using the same $[MoS_4]^{2-}$ precursor solution.[21,22] This method employs the photogenerated electrons within the semiconductor conduction band as a potent reducing agent to convert the $[MoS_4]^{2-}$ precursor into the *a*-MoS_x catalyst, which is subsequently self-assembled onto the semiconductor surface. Here we show the application of this deposition methodology to grow amorphous cobalt molybdenum sulfide (denoted hereafter as *a*-$CoMoS_x$) onto the surface of Si. This heterobimetallic sulfide catalyst is more active in HER compared to the *a*-MoS_x.[23] The resultant Si/*a*-$CoMoS_x$ photocathode shows impressive photocatalytic activities, which are among the best reported performances for noble-metal-free Si electrodes. Because the *a*-$CoMoS_x$ catalyst is active over a wide range of pH values, the Si/*a*-$CoMoS_x$ photocathode can be used to generate H_2 in different pH solutions. This property makes Si/*a*-$CoMoS_x$ a promising candidate for incorporation as a photocathode into a complete PEC device for the solar-driven water splitting.

RESULTS AND DISCUSSION

We first revisited the electrodeposition and reinvestigated the catalytic activities of *a*-$CoMoS_x$. It was found that the deposition of *a*-$CoMoS_x$ occurs at a significantly higher rate compared to that of *a*-MoS_x irrespective of applied potential: both cathodic (Supporting Information Figure S1) and anodic potentials (Figure S2). Thus, by employing the identical dynamic potential cycling deposition conditions, as those described by Hu and co-workers,[23] the amount of *a*-$CoMoS_x$ deposited was considerably higher than that of *a*-MoS_x counterpart (Figure S3). This means that careful considerations about catalyst loading are needed when comparing the intrinsic activities of these materials.

Here, we show catalytic activities of *a*-$CoMoS_x$ *versus* *a*-MoS_x, both obtained *via* cathodic deposition, because it is relevant to the photoassisted electrodeposition of these catalysts on a Si electrode (see below). A film of *a*-$CoMoS_x$ was deposited on a carbon disk electrode from a 0.25 mM $[Co(MoS_4)_2]^{2-}$ solution by applying a constant cathodic potential of −0.3 V *vs* NHE. The carbon electrode was held at −0.5 V *vs* NHE for the deposition of an *a*-MoS_x film from a 0.5 mM $[MoS_4]^{2-}$ solution. In order to deduce the intrinsic catalytic activities of *a*-$CoMoS_x$ and *a*-MoS_x, electrodes having similar loadings (in the range of 3.7×10^{-7} to 3.7×10^{-6} mol cm^{-2}) were assayed.[24] We found that, irrespective of catalyst loadings, *a*-$CoMoS_x$ electrodes displayed catalytic activities significantly higher than those of the *a*-MoS_x counterpart (Figure S4). In a pH 7 phosphate buffer solution (1.0 M), the *a*-$CoMoS_x$ electrode with a loading of 3.6×10^{-6} mol cm^{-2} displays an onset overpotential η of ∼100 mV, an exchange current density j_0 of 0.155 mA cm^{-2}, and a Tafel slope of 67 mV $decade^{-1}$. The Tafel slope, obtained from steady-state measurements (see Supporting Information for details), was found to be increased in diluted phosphate buffer solutions (Figure S5). It suggests potential involvement of phosphates within the catalysis. Analysis performed on the *a*-$CoMoS_x$ electrode after catalysis turnover did not reveal any surface binding phosphate species. Thus, the role of the phosphate anion is likely limited to accelerate the transportation of protons from the bulk solution to the catalytic site. Irrespective of phosphate concentrations, pH titrations showed a dependence of ∼60 mV pH^{-1} for the external potential required for the *a*-$CoMoS_x$ electrode to sustain a constant catalytic current (Figure S6). These results show that the catalytic H_2 generation is limited by a $1H^+$, $1e^-$ process.[25] This finding seems to be a general property for molybdenum/tungsten-based sulfide catalysts as it has also been observed for *a*-$CoWS_x$ and *a*-MoS_x materials.[11]

Having established the high catalytic activity of *a*-$CoMoS_x$ for HER, we investigated the possibility of using it to decorate the surface of Si electrodes to investigate their photocatalytic capability. For comparison, Si/*a*-MoS_x electrodes were also prepared under comparable conditions. The Si electrodes employed (geometric size of 2.0×1.0 cm^2) were prepared from available boron-doped Si(100) wafers (Silicon Valley Microelectronics). Prior to use, the Si electrodes were carefully treated with $NH_4H{\cdot}HF$ buffer solution to remove the SiO_2 native layer. The back contact was then made with a Au layer (∼60 nm thickness), prepared *via* thermal evaporation. The exposed working area was limited to be 0.25 cm^2 by covering the nonactive surface of the electrode (including the edge electrode) with chemically stable epoxy resin (Figure 1a). As expected, this bare planar Si electrode generates limited photocurrents when immersed in a pH 7 phosphate buffer solution because of the slow charge transfer at the Si/phosphate electrolyte interface (Figure 1c, blue trace). Adding 0.5 mM $[MoS_4]^{2-}$ significantly enhances the charge transfer, which can now occur at the Si/$[MoS_4]^{2-}$ junction (Figure 1c, brown trace). Charge injection from the illuminated Si electrode results in the reduction of $[MoS_4]^{2-}$, producing *a*-MoS_x, which is subsequently self-assembled onto the Si electrode surface (Figure 1b). Interestingly, as found in the dark cathodic deposition on a carbon disk electrode (see Supporting Information Figure S1), the photoassisted electrodeposition of *a*-$CoMoS_x$ on a Si electrode occurs at a more positive potential than that of *a*-MoS_x deposition: −0.05 or −0.25 V *vs* NHE (Figure 1c, red trace). When 0.25 mM $[Co(MoS_4)_2]^{2-}$ solution was employed, deposition of an *a*-$CoMoS_x$ film was readily accomplished by holding the Si

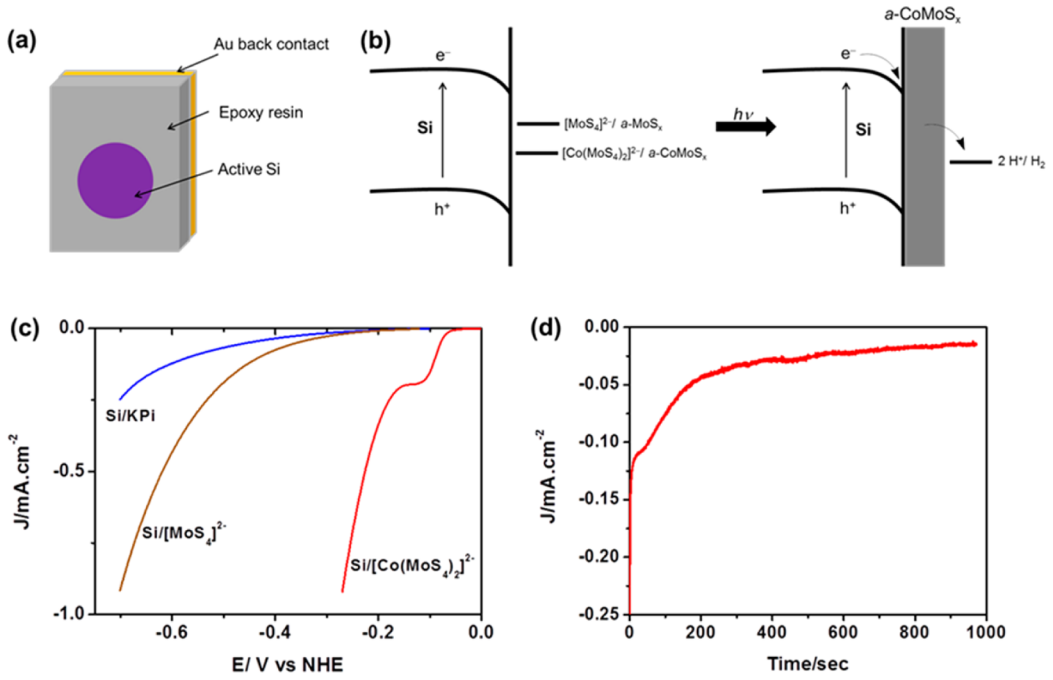

Figure 1. (a) Diagrammatic drawing of a Si working electrode. (b) Schematic presentation of the photoassisted electrodeposition process adopted to prepare Si/*a*-$CoMoS_x$ and Si/*a*-MoS_x electrodes and how these cathodes become photoactive for HER. (c) Polarization curves recorded on a Si electrode immersed in pH 7 electrolyte without (blue trace) and with 0.5 mM $[MoS_4]^{2-}$ (brown trace) and 0.25 mM $[Co(MoS_4)_2]^{2-}$ (red trace). (d) Deposition curve of an *a*-$CoMoS_x$ film on a Si electrode at an applied bias of −0.15 V *vs* NHE.

electrode at a constant potential of −0.15 V *vs* NHE and under standard 1 sun illumination (Figure 1d). The thickness of a deposited *a*-$CoMoS_x$ film can be easily monitored by controlling the total deposition charges (Figure S7). More negative bias of −0.4 V *vs* NHE was applied for deposition of an *a*-MoS_x film.

We examined the morphology and chemical composition of deposited *a*-$CoMoS_x$ films by means of scanning electron microscopy (SEM) and X-ray photoelectron spectroscopy (XPS). Panels a and b of Figure 2 show a cross-section observation and surface morphology of a ∼90 nm *a*-$CoMoS_x$ film obtained by passing a total deposition charge density of 52 mC cm^{-2} (thus corresponding to a catalyst loading of 2.7 × 10^{-7} mol cm^{-2}). The *a*-$CoMoS_x$ film is made of nanoparticles of ∼100 nm diameter size and displays porous morphology with high specific surface area, which is expected to be beneficial to produce high catalytic activities. Furthermore, the cross-section analysis revealed that the *a*-$CoMoS_x$ film is conformal and perfectly covers the Si electrode surface. This factor is believed to be critical to protect the Si electrode against oxidation and make it suitable for long run applications. XPS analysis reveals the complex heterobimetallic sulfide nature of the *a*-$CoMoS_x$ film: Co $2p_{3/2}$ was found at 778.94 eV (Figure 2c), being very close to that reported for the cobalt molybdenum sulfide phase (CoMoS, 778.64 eV).[26] The presence of cobalt sulfides such as Co_9S_8 (Co $2p_{3/2}$ 778.09 eV)[26] and cobalt oxides (CoO, 780.0 eV) or hydroxides ($Co(OH)_2$, 780.4 eV; CoOOH, 780.1 eV) can be excluded.[27] The Mo 3d envelope can be fitted into three species with different chemical environments (Figure 2d). The Mo $3d_{5/2}$ 228.67 eV species is assigned to $Mo^{IV}S_x$, while higher species of Mo $3d_{5/2}$ 229.87 eV is attributed to molybdenum oxysulfide type $Mo^{V}OS_x$.[26] Some MoO_3 impurities (Mo $3d_{5/2}$ 232.32 eV) were also found. Analysis of the S 2p envelope reveals the presence of both monosulfide S^{2-} (S $2p_{3/2}$ 161.25 and 161.71 eV) and disulfide $(S-S)^{2-}$ ligands (S $2p_{3/2}$ 162.8 eV) (Figure 2e). The film stoichiometry is $Co_{0.54}MoS_{4.14}$. We note that this as-prepared film has a cobalt content higher than that obtained by employing the dynamic potential deposition method (Co/Mo = 0.29:1).[23] However, under H_2 photoproduction conditions, the cobalt content was found to be lowered, indicating that the *a*-$CoMoS_x$ catalyst was partially corroded or dissolved as has been observed for the cobalt-free *a*-MoS_x catalyst.[8] The steady-state catalyst film under turnover conditions was determined to be $Co_{0.26}MoS_{2.63}$. The analysis of the Si/*a*-$CoMoS_x$ electrode after being held at 0 V *vs* RHE, in a pH 4.25 phosphate solution for 1 h under 1 sun illumination, also revealed an increase of the MoO_3 content from 18 to 24% of the total Mo 3d signal (Figure S8). This oxidation can occur during the H_2 photoproduction process and/or because of air contact during the sample handling prior to loading in the spectrometer. Remarkably, the *a*-$CoMoS_x$ catalyst layer efficiently protects against the oxidation of the Si surface. In fact, we observed similar, if not lower, Si−O

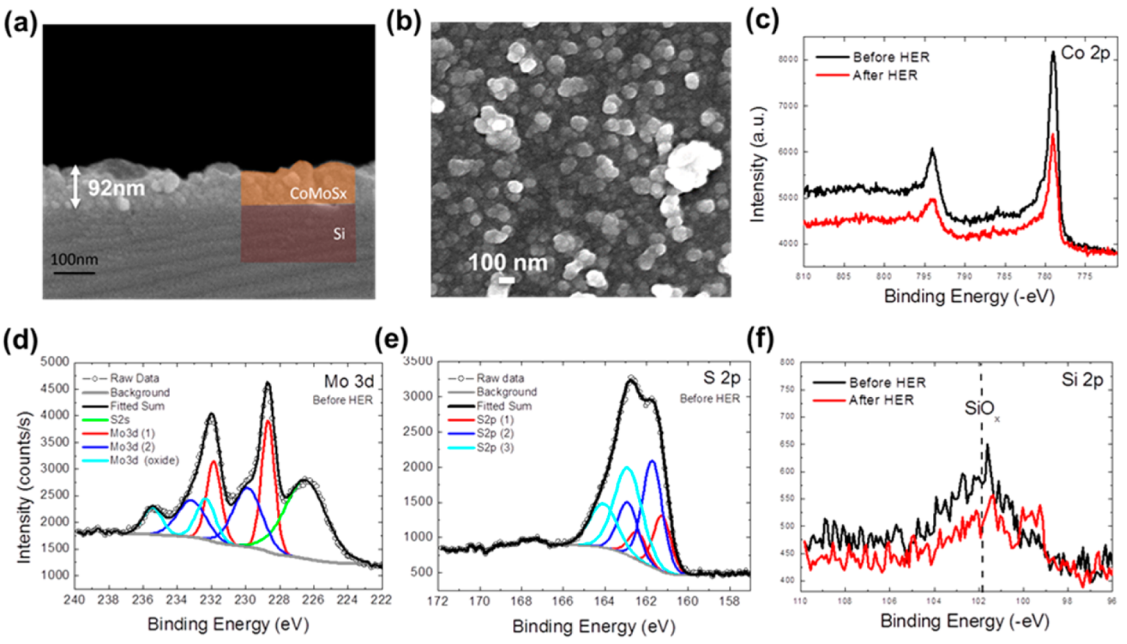

Figure 2. Characterizations of the Si/*a*-CoMoS$_x$ electrode with a catalyst loading of 2.7 × 10^{-7} mol *a*-CoMoS$_x$ cm^{-2}. (a) Cross section and (b) surface plane view taken by SEM. (c−f) Elemental analysis by X-ray photoelectron spectroscopy carried out on the as-prepared electrode and the same electrode after being held for 1 h under H$_2$ photogeneration conditions: external bias of 0 V *vs* RHE, pH 4.25 phosphate electrolyte solution, and 1 sun light illumination. For clarification, Mo 3d and S 2p spectra collected on the electrode after H$_2$ generation are presented in Supporting Information Figure S8.

peak intensities for the Si/*a*-CoMoS$_x$ electrode after functioning (Figure 2f).

Protection to the Si surface is apparently less efficient with lower catalyst loadings. Thinner *a*-CoMoS$_x$ film of ∼40 nm gives an incomplete coverage on the Si surface with some exposed pinholes (Figure S9). Furthermore, less catalyst loading implies lower available catalytic centers for the proton reduction. By contrast, thick *a*-CoMoS$_x$ films would block or reduce light absorption by the Si electrode because the catalytic films have absorptions at λ_{max} 600, 470, 400, and 320 nm (Figure S10). Therefore, we optimized the thickness of the *a*-CoMoS$_x$ catalytic layer in order to achieve the best performance for a Si/*a*-CoMoS$_x$ photoelectrode. Figure 3a shows *I*−*V* curves recorded under standard 1 sun illumination in a pH 4.25 phosphate solution employing Si/*a*-CoMoS$_x$ photoelectrodes having different *a*-CoMoS$_x$ loadings. These electrodes display comparable onset potential for photocurrent generation (open circuit voltage V_{OC} of ∼0.25 V *vs* RHE). By contrast, photocurrents generated at a given bias clearly depend on catalyst loading. We use the catalytic current j_{sc} measured at a potential of 0 V *vs* RHE as a key factor to judge the performance of these electrodes. Plotting j_{sc} *versus* *a*-CoMoS$_x$ loadings shows a Volcano plot shape (Figure 3b). The best performance was achieved with a Si/*a*-CoMoS$_x$ electrode having a catalyst loading of 2.7 × 10^{-7} mol cm^{-2} (corresponding to a ∼90 nm *a*-CoMoS$_x$ layer whose morphology and cross-section analysis are shown in Figure 2a,b). This electrode displays j_{sc} of 17.5 mA cm^{-2}. Bulk photoelectrolysis performed by holding this electrode at 0 V *vs* RHE for 3 h showed relatively stable photocurrent with current-to-hydrogen yield determined to be close to unity (Figure 3c,d). To the best of our knowledge, the current Si/*a*-CoMoS$_x$ performance is among the best reported for Si photocathodes decorated with noble-metal-free HER catalysts (Table 1, entries 1−7). However, the achieved j_{sc} and $j_{plateau}$ (light-limited photocurrent) are still lower than the theoretically predicted photocurrent of 44 mA cm^{-2} for the Si electrode.[2] Further performance improvement is possible by implementing an n$^+$ emitter layer, which is expected to help improve charge separation within the Si electrode, as illustrated in the literature (Table 1, entries 8−12).

The charge transfer within Si photoelectrodes under H$_2$ generation conditions was examined by means of electrochemical impedance spectroscopy analyses. Bare Si, Si/*a*-CoMoS$_x$, and Si/*a*-MoS$_x$ electrodes (both *a*-CoMoS$_x$ and *a*-MoS$_x$ loaded at 2.7 × 10^{-7} mol cm^{-2}) were held in pH 4.25 phosphate electrolyte solution under standard 1 sun illumination. The bare Si electrode shows a single arc corresponding to the direct charge transfer to the electrolyte, which can be fitted with a simple series resistance (R_s) and capacitance (C_{bulk}) in parallel to a charge transfer resistance (R_{ct}) (Figure 4a, blue trace). In contrast, the Nyquist plots at different applied potentials of Si with *a*-MoS$_x$ and *a*-CoMoS$_x$ loadings followed the previously reported trend of charge transfer through intermediate states (Figure 4a,b, brown and red traces).[16,29] These results

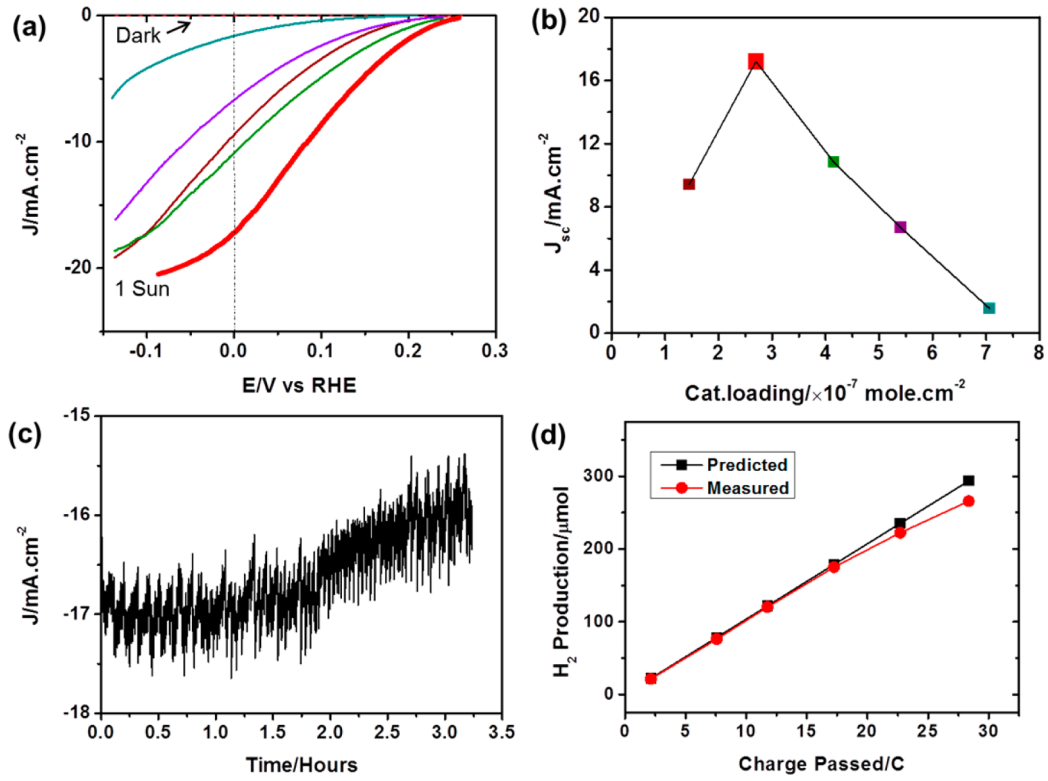

Figure 3. (a) Performance assayed in pH 4.25 phosphate solution under standard 1 sun illumination of Si/*a*-$CoMoS_x$ photocathodes having different catalyst loadings. Potential scan rate was 10 mV s^{-1}. Color code: brown, 1.5 × 10^{-7}; red, 2.7 × 10^{-7}; blue, 4.7 × 10^{-7}; olive, 5.6 × 10^{-7}; black, 7.3 × 10^{-7} mol *a*-$CoMoS_x$ cm $^{-2}$. (b) Plotting j_{sc} at RHE 0 V *versus* catalyst loadings. (c) Bulk photoelectrolysis at 0 V *vs* RHE and under 1 sun illumination employing the best Si/*a*-$CoMoS_x$ photocathode. (d) Theoretical calculated and measured H_2 amount during the bulk photoelectrolysis.

TABLE 1. Photocatalytic Performance of Selected Si Photocathodes Decorated with Noble-Metal-Free HER Catalyst[a]

entry	electrode	V_{OC} (V *vs* RHE)	j_{sc} (mA cm^{-2})	$j_{plateau}$ (mA cm^{-2})	catalyst deposition	refs
1	Si/*a*-$CoMoS_x$	0.25	17.5	20	photoassisted deposition	this work
2	Si/*a*-MoS_x	0.2	6.0		photoassisted deposition	this work
3	Si/$[Mo_3S_4]^{4+}$	0.15	8	12	drop-casting	15
4	Si/1T-MoS_2	0.2	9.2	14.3	drop-casting	16
5	Si/1T-MoS_2	0.25	17.6	26.7	CVD	16
6	Si/NiMo	0.15	15	20	electrodeposition	4
7	Si MWs/NiMo	0.14	6.7		electrodeposition	28
8	p/n$^+$Si/Ti/*a*-MoS_x	0.33	16	16	electrodeposition	17
9	p/n$^+$Si/Mo/MoS_2/*a*-MoS_x	0.35	12	12	sulfurization of Mo substrate	5
10	p/n$^+$Si/Mo/MoS_2	0.32	17.5	17.5	sulfurization Mo of Mo substrate	18
11	p/n$^+$Si/Mo/MoS_2/$[Mo_3S_{13}]^{2-}$	0.4	17.5	17.5	drop-casting	18
12	p/n$^+$ Si MWs/NiMo	0.485	10.3	10.3	electrodeposition	28

[a] Note, j_{sc} is the catalytic current measured at an applied bias of 0 V *vs* RHE; $j_{plateau}$ is the light-limited photocurrent; 1T-MoS_2 is the metallic crystalline molybdenum disulfide; n$^+$ is the phosphorus-doped Si emitter layer; Si MWs are microarray silicon; CVD is chemical vapor deposition.

can be fitted with the equivalent circuit shown in Figure 4c, where R_s is the series resistance, C_{bulk} is the capacitance of the Si, C_{trap} is the capacitance of the catalyst, $R_{trapping}$ is the resistance of the charge transfer from the Si to the catalyst, and $R_{ct,trap}$ is the resistance of the charge transfer from the catalyst to the electrolyte that induces the H_2 generation. This fitting clearly demonstrates that the *a*-$CoMoS_x$ and *a*-MoS_x catalyst layers act as mediators that help to promote the electron transfer between illuminated Si and electrolyte with the concomitant evolution of H_2. As seen in Figure 4d, $R_{trapping}$ for the *a*-$CoMoS_x$ sample is about 1 order of magnitude smaller than that for the *a*-MoS_x counterpart, indicating that the former is more efficient at quenching electrons derived from the illuminated Si. Moreover, because of its enhanced catalytic activities, the *a*-$CoMoS_x$ catalyst uses these electrons more efficiently to generate H_2 compared to the *a*-MoS_x catalyst. Indeed, $R_{ct,trap}$ values of about 1 order smaller were measured for the *a*-$CoMoS_x$ catalyst irrespective of

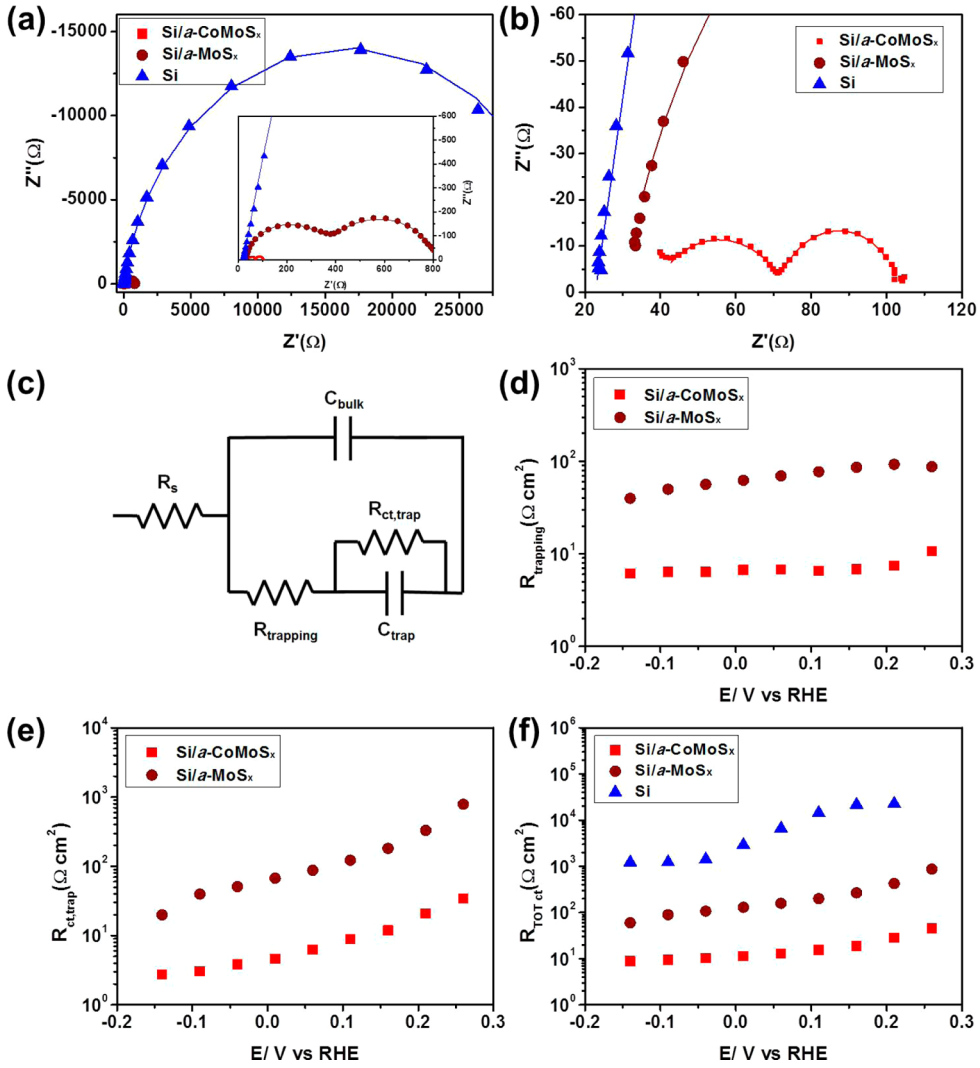

Figure 4. (a,b) Example of Nyquist plots of Si electrodes without and with *a*-MoS_x or *a*-$CoMoS_x$ catalyst decorated. Measurements were carried out at applied bias of 0 V *vs* RHE under 1 sun illumination. The solid lines correspond to the fitting to the respective equivalent circuit. (c) Equivalent circuit corresponding to the charge transfer from the Si to the electrolyte through a catalyst. (d) Charge transfer resistance $R_{trapping}$ from illuminated Si to the catalyst layer. (e) Charge transfer resistance $R_{ct,trap}$ from the catalyst layer to the electrolyte to generate H_2. (f) Total charge transfer resistance for Si electrodes with and without catalysts.

applied bias (Figure 4e). We assume that the actual H_2 production rate is reflected by the sum of $R_{trapping}$ and $R_{ct,trap}$. This total resistance (impedance) is found to be smaller for the Si/*a*-$CoMoS_x$ electrode compared to the Si/*a*-MoS_x (Figure 4f). This result clearly explains the significantly enhanced performance of the Si/*a*-$CoMoS_x$ electrode (Table 1 and Supporting Information Figure S11). We also note that, without catalyst present, the direct charge transfer from illuminated Si to the electrolyte is extremely unfavorable as evidenced by high R_{ct} resistance that is about 2 orders of magnitude higher compared with the total $R_{trapping} + R_{ct,trap}$ of the Si/*a*-$CoMoS_x$ electrode.

CONCLUSION

We report herein a facile, scalable process to fabricate a noble-metal-free Si/*a*-$CoMoS_x$ hybrid photocathode for solar hydrogen generation. Within this electrode, the *a*-$CoMoS_x$ catalyst layer traps photogenerated electrons and subsequently transfers these electrons to the electrolyte by an efficiently catalytic mechanism resulting in H_2 generation. Compared with *a*-MoS_x, the *a*-$CoMoS_x$ layer displays better electron-accepting properties as well as enhanced HER catalytic activity. Therefore, as a consequence, the Si/*a*-$CoMoS_x$ electrode shows significant enhanced performance compared with a Si/*a*-MoS_x equivalent. Indeed, the Si/*a*-$CoMoS_x$ electrode described here is among the best Si photocathodes decorated with noble-metal-free catalysts that have been reported to date. Furthermore, this Si/*a*-$CoMoS_x$ is perfectly active over a wide range of pH values (Figure S12), making it a promising candidate as a photocathode to be assembled together with an

appropriate photoanode, such as $BiVO_4$,[30] for engineering a complete dual light absorbing tandem photoelectrochemical cell for a solar-driven water splitting application.

METHODS

p-Si Electrode Preparation. A boron-doped p-type Si(100) wafer (525 ± 25 μm thickness, resistivity of 10−20 Ω·cm) was purchased from Silicon Valley Microelectronics. Si working electrodes were cut from wafers at 1 × 2 cm^2 size. A diamond pen was used to scratch the back side of the Si electrode to create a rough surface, which is found to be critical for deposition of a Au back contact layer. Prior to use, Si electrodes were cleaned by subsequent sonication in water, acetone, and ethanol. The native SiO_2 layer on the Si electrode surface was then removed by sonicating the electrodes in a 5 wt % NH_4F·HF solution for 30 min. The Si electrodes were then rinsed in degassed deionized water and dried under a stream of N_2.

The backside Ohmic contact was made by depositing a layer of Au (~60 nm thickness) by means of a thermal evaporator.

The Si working area was limited to be ~0.25 cm^2 by covering the unexposed area (including the Si edges) with chemically stable epoxy resin. The electrode was then kept in a glovebox filled with Ar gas.

Photoassisted Deposition of *a*-$CoMoS_x$. A deposition bath consisting of 0.25 mM $[Co(MoS_4)_2](NH_4)_2$ was prepared by adding 0.25 mM $Co(NO_3)_2$ into 0.5 mM $[MoS_4](NH_4)_2$ freshly prepared solution in pH 7 phosphate buffer (0.1 M). Si electrodes were then held in this solution at an external bias of −0.15 V *vs* NHE under standard 1 sun illumination. During the deposition process, the solution was stirred with the aid of a magnetic stirrer. The resultant Si/*a*-$CoMoS_x$ was carefully washed with degassed water and ethanol and dried under an Ar stream. Freshly prepared Si/*a*-$CoMoS_x$ electrodes were employed for assaying photocatalytic performance and electrochemical impedance spectroscopy analysis. These electrodes were kept under Ar prior to be use in microscopic and chemical composition analyses.

Comparable conditions were employed for preparing Si/*a*-MoS_x electrodes using a deposition bath consisting of 0.5 mM $[MoS_4](NH_4)_2$ dissolved in 0.1 M phosphate buffer solution.

Performance Assays. Photocatalytic properties of Si electrodes were assayed in a pH 4.25 phosphate electrolyte degassed by Ar. The light source was standard 1 sun illumination. A customized three-electrode, two-compartment electrochemical cell was employed. The reference electrode was Ag/AgCl/3 M KCl, and the counter electrode was a Pt wire. *I*−*V* curves were recorded by linear sweep voltammetry at a potential scan rate of 10 mV s^{-1} from the cathodic to anodic potential and finished at an open circuit potential to avoid Si oxidation. Potentials were quoted against the normal hydrogen electrode (NHE, $E_{vs\ NHE} = E_{vs\ Ag/AgCl} + 0.21$ V) or the reversible hydrogen electrode (RHE, $E_{vs\ RHE} = E_{vs\ Ag/AgCl} + 0.21 + 0.059 \times$ pH V). The electrochemical impedance spectroscopy measurements were carried out using a potentiostat (Methrohm-Autolab, AUT 83285). A potential perturbation (10 mV) was applied at varying dc voltages with a frequency sweep from 200 kHz to 0.1 Hz. The impedance data were fitted by Z-view software.

Conflict of Interest: The authors declare no competing financial interest.

Acknowledgment. Y.C. acknowledges the Energy Research Institute @ Nanyang Technological University (ERI@N) for a Ph. D. scholarship. P.D.T., L.H.W., and J.B. acknowledge the Energy Research Institute @ Nanyang Technological University (ERI@N) and the Singapore−Berkeley Research Initiative for Sustainable Energy (SinbeRISE) CREATE for financial and facility support.

Supporting Information Available: Experimental details. Dark electrodeposition and electrochemical properties of *a*-MoS_x and *a*-$CoMoS_x$ catalysts. Morphology, chemical composition, and performance of Si photoelectrodes. This material is available free of charge *via* the Internet at http://pubs.acs.org.

REFERENCES AND NOTES

1. Hu, S.; Xiang, C.; Haussener, S.; Berger, A. D.; Lewis, N. S. An Analysis of the Optimal Band Gaps of Light Absorbers in Integrated Tandem Photoelectrochemical Water-Splitting Systems. *Energy Environ. Sci.* **2013**, *6*, 2984–2993.
2. Chen, Z.; Jaramillo, T. F.; Deutsch, T. G.; Kleiman-Shwarsctein, A.; Forman, A. J.; Gaillard, N.; Garland, R.; Takanabe, K.; Heske, C.; Sunkara, M.; et al. Accelerating Materials Development for Photoelectrochemical Hydrogen Production: Standards for Methods, Definitions, and Reporting Protocols. *J. Mater. Res.* **2010**, *25*, 3–16.
3. Boettcher, S. W.; Warren, E. L.; Putman, M. C.; Santori, E. A.; Turner-Evans, D.; Kelzenberg, M. D.; Walter, M. G.; McKone, J. K.; Brunschwig, B. S.; et al. Photoelectrochemical Hydrogen Evolution Using Si Microwire Arrays. *J. Am. Chem. Soc.* **2011**, *133*, 1216–1219.
4. McKone, J. R.; Warren, E. L.; Bierman, M. J.; Boettcher, S. W.; Brunschwig, B. S.; Lewis, N. S.; Gray, H. B. Evaluation of Pt, Ni, and Ni−Mo Electrocatalysts for Hydrogen Evolution on Crystalline Si Electrodes. *Energy Environ. Sci.* **2011**, *4*, 3573–3583.
5. Laursen, A. B.; Pedersen, T.; Malacrida, P.; Seger, B.; Hansen, O.; Vesborg, P. C.; Chorkendorff, Ib. MoS_2: An Integrated Protective and Active Layer on n(+)p-Si for Solar H_2 Evolution. *Phys. Chem. Chem. Phys.* **2013**, *15*, 20000–20004.
6. Jaramillo, T. F.; Jorgensen, K. P.; Bonde, J.; Nielsen, J. H.; Horch, S.; Chorkendorff, Ib. Identification of Active Edge Sites for Electrochemical H_2 Evolution from MoS_2 Nanocatalysts. *Science* **2007**, *317*, 100–102.
7. Kibsgaard, J.; Chen, Z.; Reinecke, B. N.; Jaramillo, T. F. Engineering the Surface Structure of MoS_2 To Preferentially Expose Active Edge Sites for Electrocatalysis. *Nat. Mater.* **2012**, *11*, 963–969.
8. Merki, D.; Fierro, S.; Vrubel, H.; Hu, X. Amorphous Molybdenum Sulfide Films as Catalysts for Electrochemical Hydrogen Production in Water. *Chem. Sci.* **2011**, *2*, 1262–1267.
9. Voiry, D.; Yamaguchi, H.; Li, J.; Silva, R.; Alves, D. C. B.; Fujita, T.; Chen, M.; Asefa, T.; Eda, G.; et al. Enhanced Catalytic Activity in Strained Chemically Exfoliated WS_2 Nanosheets for Hydrogen Evolution. *Nat. Mater.* **2013**, *12*, 850–855.
10. Tran, P. D.; Nguyen, M.; Paramana, S. S.; Bhattacharjee, A.; Chiam, S. Y.; Fize, J.; Field, M. J.; Artero, V.; Wong, L. H.; Loo, J.; et al. Copper Molybdenum Sulfide: A New Efficient Electrocatalyst for Hydrogen Production from Water. *Energy Environ. Sci.* **2012**, *5*, 8912–8916.
11. Tran, P. D.; Chiam, S. Y.; Boix, P. P.; Ren, Y.; Paramana, S. S.; Fize, J.; Artero, V.; Barber, J. Novel Cobalt/Nickel−Tungsten−Sulfide Catalysts for Electrocatalytic Hydrogen Generation from Water. *Energy Environ. Sci.* **2013**, *6*, 2452–2459.
12. Sun, Y.; Liu, C.; Grauer, D. C.; Yano, J.; Long, J. R.; Yang, P.; Chang, C. J. Electrodeposited Cobalt−Sulfide Catalyst for Electrochemical and Photoelectrochemical Hydrogen Generation from Water. *J. Am. Chem. Soc.* **2013**, *135*, 17699–17702.
13. Vrubel, H.; Hu, X. Growth and Activation of an Amorphous Molybdenum Sulfide Hydrogen Evolving Catalyst. *ACS Catal.* **2013**, *3*, 2002–2011.
14. Morales-Guio, C. G.; Hu, X. Amorphous Molybdenum Sulfides as Hydrogen Evolution Catalysts. *Acc. Chem. Res.* **2014**, *47*, 2671–2681.
15. Hou, Y.; Abrams, B. L.; Vesborg, P. C. K.; Bjorketun, M. E.; Herbst, K.; Bechi, L.; Setti, A. M.; Damsgaard, C. D.; Pedersen, T.; Hansen, O.; et al. Bioinspired Molecular Co-catalysts Bonded to a Silicon Photocathode for Solar Hydrogen Evolution. *Nat. Mater.* **2011**, *10*, 434–438.

16. Ding, Q.; Meng, F.; English, C. R.; Caban-Acevedo, M.; Shearer, M. J.; Liang, D.; Daniel, A. S.; Hamer, R. J.; Jin, S. Efficient Photoelectrochemical Hydrogen Generation Using Heterostructures of Si and Chemically Exfoliated Metallic MoS_2. *J. Am. Chem. Soc.* **2014**, *136*, 8504–8507.
17. Seger, B.; Lausen, A. B.; Vesborg, P. C. K.; Pedersen, T.; Hansen, O.; Dahl, S.; Chorkendorff, Ib. Hydrogen Production Using a Molybdenum Sulfide Catalyst on a Titanium-Protected n+p-Silicon Photocathode. *Angew. Chem., Int. Ed.* **2012**, *51*, 9128–9131.
18. Benck, J. D.; Lee, S. C.; Fong, K. D.; Kibsgaard, J.; Sinclair, R.; Jaramillo, T. F. Designing Active and Stable Silicon Photocathodes for Solar Hydrogen Production Using Molybdenum Sulfide Nanomaterials. *Adv. Energy Mater.* **2014**, *4*, 1400739.
19. Bélanger, D.; Laperriére, G.; Marsan, B. The Electrodeposition of Amorphous Molybdenum Sulfide. *J. Electroanal. Chem.* **1993**, *347*, 165–183.
20. Ponomarev, E. A.; Neumann-Spallart, M.; Hodes, G.; Lévy-Clément, C. Electrochemical Deposition of MoS_2 Thin Films by Reduction of Tetrathiomolybdate. *Thin Solid Films* **1996**, *280*, 86–89.
21. Tran, P. D.; Pramana, S. S.; Kale, V. S.; Nguyen, M.; Chiam, S. Y.; Batabyal, S. K.; Wong, L. H.; Barber, J.; Loo, J. Novel Assembly of an MoS_2 Electrocatalyst onto a Silicon Nanowire Array Electrode To Construct a Photocathode Composed of Elements Abundant on the Earth for Hydrogen Generation. *Eur. J. Chem.* **2012**, *18*, 13994–13999.
22. Nguyen, M.; Tran, D. P.; Pramana, S. S.; Lee, R. L.; Batabyal, S. K.; Mathews, N.; Wong, L. H.; Graetzel, M. *In Situ* Photoassisted Deposition of MoS_2 Electrocatalyst onto Zinc Cadmium Sulphide Nanoparticle Surfaces to Construct an Efficient Photocatalyst for Hydrogen Generation. *Nanoscale* **2013**, *5*, 1479–1482.
23. Merki, D.; Vrubel, H.; Rovelli, L.; Fierro, S.; Hu, X. Fe, Co, and Ni Ions Promote the Catalytic Activity of Amorphous Molybdenum Sulfide Films for Hydrogen Evolution. *Chem. Sci.* **2012**, *3*, 2515–2525.
24. We assume that both *a*-$CoMoS_x$ and *a*-MoS_x depositions are two-electron reduction processes (please also refer to the Supporting Information for details).
25. Costentin, C.; Robert, M.; Savéant, J.-M. Update 1 of: Electrochemical Approach to the Mechanistic Study of Proton-Coupled Electron Transfer. *Chem. Rev.* **2010**, *110*, PR1–PR40.
26. Gandubert, A. D.; Legens, C.; Guillaume, D.; Rebours, S.; Payen, E. X-ray Photoelectron Spectroscopy Surface Quantification of Sulfided CoMoP Catalysts—Relation between Activity and Promoted Sites—Part I: Influence of the Co/Mo Ratio. *Oil Gas Sci. Technol.* **2007**, *62*, 79–89.
27. Biesinger, M. C.; Payne, B. P.; Grosvenor, A. P.; Lau, L. W. M.; Gerson, A. R.; Smart, R. S. C. Resolving Surface Chemical States in XPS Analysis of First Row Transition Metals, Oxides and Hydroxides: Cr, Mn, Fe, Co and Ni. *Appl. Surf. Sci.* **2011**, *257*, 2717–2730.
28. Warren, E. L.; McKone, J. R.; Atwater, H. A.; Gray, H. B.; Lewis, N. S. Hydrogen-Evolution Characteristics of Ni–Mo-Coated, Radial Junction, n+p-Silicon Microwire Array Photocathodes. *Energy Environ. Sci.* **2012**, *5*, 9653–9661.
29. Klahr, B.; Gimenez, S.; Fabregat-Santiago, F.; Hamann, T.; Bisquert, J. Water Oxidation at Hematite Photoelectrodes: The Role of Surface States. *J. Am. Chem. Soc.* **2012**, *134*, 4294–4302.
30. Eisenberg, D.; Ahn, H. S.; Bard, A. J. Enhanced Photoelectrochemical Water Oxidation on Bismuth Vanadate by Electrodeposition of Amorphous Titanium Dioxide. *J. Am. Chem. Soc.* **2014**, *136*, 14011–14014.